Two distinct activity patterns of fast-spiking interneurons during neocortical UP states

Maria Victoria Puig*†, Mika Ushimaru*‡, and Yasuo Kawaguchi*‡§

*Division of Cerebral Circuitry, National Institute for Physiological Sciences, Myodaiji, Okazaki, Aichi 444-8787, Japan; and ‡Department of Physiological Sciences, Graduate University for Advanced Studies (SOKENDAI), Okazaki, 444-8585, Japan

Edited by Edward G. Jones, University of California, Davis, CA, and approved April 7, 2008 (received for review December 26, 2007)

During sleep, neocortical neuronal networks oscillate slowly (<1 Hz) between periods of activity (UP states) and silence (DOWN states). UP states favor the interaction between thalamic-generated spindles (7–14 Hz) and cortically generated gamma (30–80 Hz) waves. We studied how these three nested oscillations modulate fast-spiking interneuron (FSi) activity *in vivo* in VGAT-Venus transgenic rats. Our data describe a population of FSi that discharge "early" within UP states and another population that discharge "late." Early FSi tended to be silent during epochs of desynchronization, whereas late FSi were active. We hypothesize that late FSi may be responsible for generating the gamma oscillations associated with cognitive processing during wakefulness. Remarkably, FSi populations were differently modulated by spindle and gamma rhythms. Early FSi were robustly coupled to spindles and always discharged earlier than late FSi within spindle and gamma cycles. The preferred firing phase during spindle and gamma waves was strongly correlated in each cell, suggesting a cross-frequency coupling between oscillations. Our results suggest a precise spatiotemporal pattern of FSi activity during UP states, whereby information rapidly flows between early and late cells, initially promoted by spindles and efficiently extended by local gamma oscillations.

gamma oscillations | local field potentials | slow-wave sleep | synchrony | thalamocortical spindles

Fast-spiking interneurons (FSi) are the most prevalent type of inhibitory neuron in the cortex and are identified by their selective expression of the calcium-binding protein parvalbumin (PV) (1, 2). Networks of electrically and chemically coupled FSi (3, 4) are involved in the generation of cortical gamma oscillations (5), which provide a critical temporal structure for cognitive processes during wakefulness such as working memory and sensory processing (6, 7). Hence, abnormalities of both FSi marker expression and gamma oscillations have been reported in some severe psychiatric disorders such as schizophrenia (8–10). Although gamma oscillations also occur during resting sleep and anesthesia, where they interact with slower cortical rhythms (11, 12), the functional role of FSi in generating gamma oscillations during sleep has not yet been established.

During early stages of sleep, gamma waves coexist with spindles within UP states. Spindle waves are slower rhythms that originate in the thalamus and are transmitted to the neocortex via a cortico-thalamo-cortical loop (13). Even as they receive highly synchronized and powerful excitatory inputs from the thalamus, experimental and modeling studies suggest that pyramidal cells discharge at a low rate during spindles. One reason for this is that, during spindling, synchronized thalamic inputs generate excitatory/inhibitory postsynaptic potential sequences in pyramidal neurons, providing them with simultaneous dendritic excitation and perisomatic inhibition, which reduces the probability of action potential generation (14, 15). Basket-cell FSi predominantly innervate the soma and proximal dendrites of pyramidal neurons (1, 16) and may account for the inhibition observed in these experiments. Other groups have found an important role for thalamic inputs in triggering neocortical recurrent activity, which is then sustained by reciprocal intracortical connections. Interneurons may play a pivotal role in shaping this process by strongly controlling excitatory activity through feedforward inhibition (17, 18). However, how excitatory thalamic inputs and FSi interact to shape cortical activity during sleep is still poorly understood.

Slow oscillations present during slow-wave sleep (SWS) are essential for memory consolidation (19, 20). It has been hypothesized that slow oscillations facilitate information transfer between the hippocampus and neocortex during sleep–wake cycles to allow consolidation of memories acquired during wakefulness (21). Consistent with this idea, hippocampal sharp-wave ripples (≈200 Hz) show strong temporal correlation with both slow (22–24) and spindle (24, 25) oscillations in the neocortex. Further, in the neocortex and hippocampus, there is simultaneous replay of spiking patterns generated earlier in the awake animal, and this process is speculated to reflect memory consolidation (26). Accordingly, during SWS, neocortical neuronal ensembles display unique patterns of discharge that repeat stereotypically in every UP state. These sequential firing patterns are independent of the direction of the propagating wave, suggesting that they arise from the local connectivity (27). However, the specific contribution of distinct neuronal populations in the generation of these sequential spiking patterns has not yet been determined.

To understand how cortical synchrony present during sleep contributes to memory encoding and consolidation, it is essential to first unravel the underlying cellular mechanisms involved in generating cortical oscillations. We examined how the activity of FSi is modulated by slow, spindle, and gamma waves during SWS and found the existence of two major firing patterns that may contribute in different ways to the generation of neocortical synchrony during natural sleep.

Results

Two Distinct Populations of FSi Discharge Early and Late During UP States. We performed single-cell juxtacellular recordings of FSi [see *Materials and Methods*, supporting information (SI) *Methods*, and Figs. S1 and S2 for details on the *in vivo* identification] in the frontal cortex of transgenic rats that coexpress the fluorescent protein Venus with the vesicular GABA transporter (VGAT). VGAT-Venus rats have fluorescent labeling of nearly all cortical GABAergic cells, including FSi (2). We recorded the activity of 50 FSi in the frontal cortex, 46 in the secondary motor

Author contributions: M.V.P. and Y.K. designed research; M.V.P. and M.U. performed research; M.V.P. and Y.K. analyzed data; and M.V.P. and Y.K. wrote the paper.

The authors declare no conflict of interest.

This article is a PNAS Direct Submission.

†To whom correspondence may be sent at the present address: The Picower Institute for Learning and Memory, Department of Brain and Cognitive Sciences, Massachusetts Institute of Technology, Cambridge, MA 02139. E-mail: mvpuig@mit.edu.

§To whom correspondence may be addressed. E-mail: yasuo@nips.ac.jp.

This article contains supporting information online at www.pnas.org/cgi/content/full/0712219105/DCSupplemental.

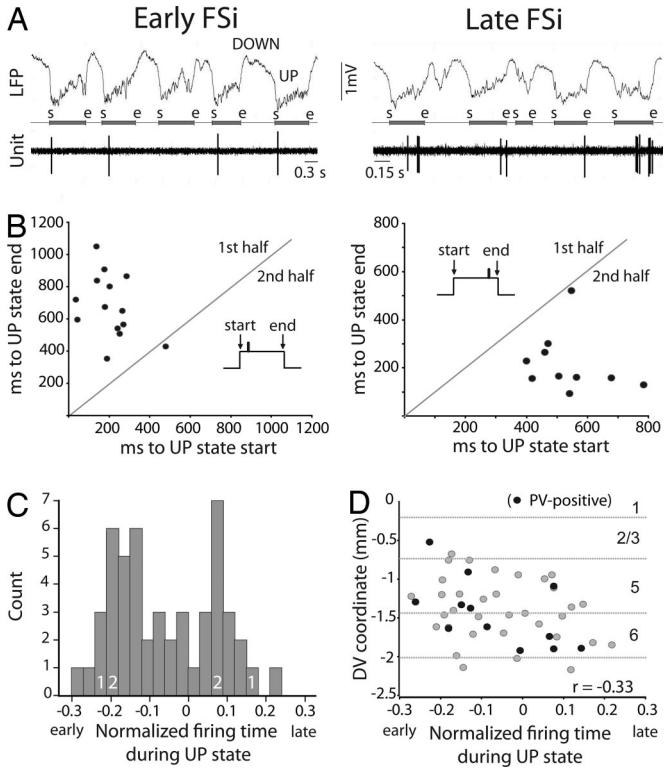

Fig. 1. FSi consistently discharge early or late during UP states. (*A*) Examples of early- and late-FSIs. The start (s) and end (e) of each UP state have been marked between the LFP and unit traces. (*B*) Scatter plots of averaged distances (in milliseconds) of all spikes within a UP state relative to the start and end of 20 consecutive UP states (same cells as in *A*). (*C*) Frequency distribution of normalized times to the start of UP states (−0.5–0.5) of all FSi recorded (n = 50). Zero indicates the center of UP state. 1 and 2 depict the location of example cells in Figs. 1 and 2, respectively. (*D*) Early units were located more superficially in the dorsoventral (DV) axis than were late units. Only cells recorded in the secondary motor area are shown (n = 46). Dashed lines depict standard layer boundaries. r correlation coefficient in all figures.

area, and 4 in the medial prefrontal cortex, and FSi firing patterns were examined during periods of SWS and desynchronization (DES).

We identified two populations of FSi based on their activity during cortical UP states. One population preferentially discharged during the first half of the UP states and were labeled "early firing." The second population discharged predominantly during the second half of the UP states and were therefore called "late-firing" (Fig. 1*A*). To quantify these tendencies, we measured the average distance (in milliseconds) of all spikes within an UP state relative to both the start and end of the UP state. Scatter plots of averaged distances to start vs. averaged distances to end (for 20 consecutive UP states) revealed the consistency of the patterns in individual FSi during SWS (Fig. 1*B*). Indeed, all neurons maintained the same relative firing pattern throughout recording sessions, sometimes up to 20 min. Next, to control for variations in UP-state duration, we normalized the position of individual spikes within UP states and averaged all distances for each unit to obtain a normalized firing time (−0.5 to 0.5, where 0 indicates the center of the UP state). Although FSi (n = 50) discharged all along the UP state, the bimodal frequency distribution suggested the existence of two major subpopulations (Fig. 1*C*). FSi with low firing rates tended to spike systematically at the beginning or end of UP states (as shown in Fig. 1) and therefore showed large normalized UP-state times. However, cells discharging trains of action potentials exhibited normalized firing times closer to 0 (Fig. S3). Interestingly, early neurons were located more superficially in the cortical layers than were late neurons, implying that, during UP states, there is a directional sequence of FSi discharge in the dorsal–ventral plane (Fig. 1*D*) (Pearson correlation, P = 0.021).

Early and Late FSi Show Brain-State-Dependent Opposing Shifts in Firing Frequency. We adjusted the level of anesthesia to allow spontaneous short-lasting epochs of DES (absence of slow waves and spindles) every ≈45 min. In 35 units, we examined changes in firing frequency between SWS and DES. Early FSi decreased their spontaneous discharge rate during DES segments, whereas late cells exhibited markedly increased activity. Identical cell-type-dependent modulation of discharge frequency was observed during both spontaneous DES occurring during periods of anesthesia and DES induced by a tail pinch (TP) delivered during anesthesia (Fig. 2*A*).

For each FSi, we compared the firing frequency of 20 consecutive UP states during SWS and 20 consecutive windows of the same duration during DES and computed a firing index (F) that measured the relative difference in discharge rate between the two brain states. F was calculated as the DES firing rate minus the SWS firing rate, divided by the sum of firing rates during both brain states. F values of 1 reflect that the cell only fired during DES (DES-active), whereas values of −1 indicate that the cell was completely silent during DES (DES-silent). Early FSi tended to be DES-silent, and late FSi tended to be DES-active (Fig. 2*C*). We hypothesize that the opposing shifts in firing frequency are reflected on every UP state but on a shorter time scale: as the UP-state/DES-epoch lengthens, early units show an ever-decreasing probability of discharge, whereas spike probability increases steadily for late units. Within cells, there was a significant correlation between F and spike timing during UP states (n = 35; $P < 0.001$). Further, the frequency distribution of F within the population appeared bimodal. Two-means cluster analysis of firing time during UP states and F index centered the two populations at −0.15 UP lag (F = −0.69) and 0.07 UP lag (F = 0.35) (Fig. 2*C*) (early, n = 22; late, n = 13; Mann–Whitney, $P < 0.001$ for both F and lag). Finally, using cluster analysis of the 35 units for which F index and UP-state firing time could be computed, we established a boundary between early and late populations that was −0.06 normalized UP-state time (dashed line in Fig. 2*C*). We then classified all FSi recorded (n = 50) into early or late patterns using this boundary and performed statistical analysis to compare the groups. The two populations displayed very similar action potential duration and amplitude but differed in their discharge frequency. Early FSi exhibited slightly higher firing rates than late FSi during SWS. However, during periods of DES, the firing rates of early units markedly decreased, whereas those of late units dramatically increased (Table 1). These results suggest that early neurons are more active during sleep, whereas late neurons likely predominate during alertness. Importantly, neurons of both patterns could be found in the same animal (n = 3 rats), demonstrating that these two populations coexist within the cortical network.

We next analyzed the bursting properties of FSi. Bursting cells show a bimodal distribution of their interspike intervals, with a first peak including the brief interspike intervals within the bursts (<10 ms) and a prominent peak at the center of the autocorrelogram (Fig. 2*B Left*). Nonbursting ("regular-spiking") neurons, have a unimodal distribution of spike intervals (28). Very few FSi spontaneously fired in bursts (n = 3 of 50 neurons, 6%, two in the secondary motor area and one in the medial prefrontal cortex). In contrast, ≈60% of identified pyramidal neurons were intrinsically bursting (Table 1). These results are in agreement with previous findings (28). Interestingly, we found that only early FSi fired in bursts (Fig. 2*B*), and

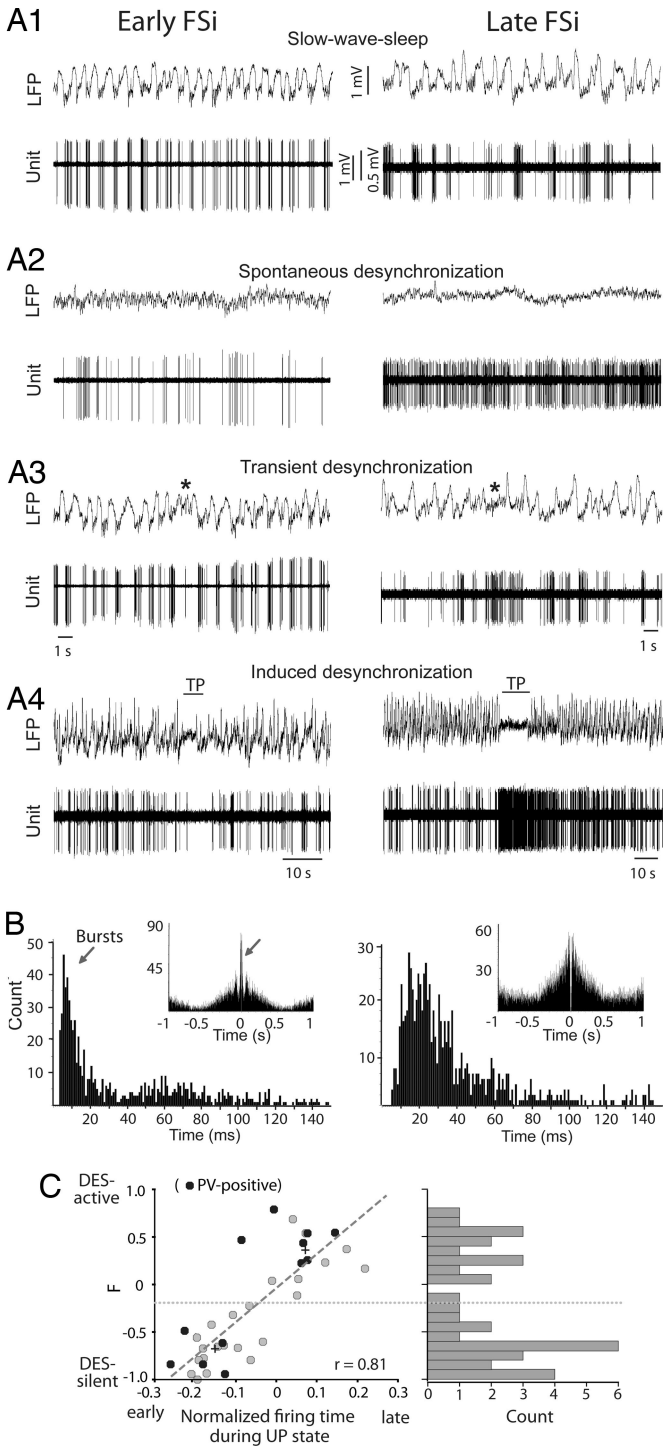

Fig. 2. Opposing shifts in discharge frequency between early and late FSi. (*A*) Examples of spontaneous firing of an early neuron and a late neuron during SWS (*A1*), DES (*A2*), transient DES occurring during SWS (*A3*), and tail pinching-induced DES (TP; *A4*) delivered during SWS. (*B*) Interspike interval histograms (ISIHs) of the cells shown in *A* during SWS epochs. Bursting units showed a bimodal distribution where the first peak contained the brief interspike intervals occurring within bursts (arrow). All bursting FSi belonged to the early FSi population (*Left*). Most FSi were regular-spiking, with ISIHs exhibiting a unimodal distribution (*Right*). (*Insets*) Autocorrelograms show high correlation for bursting cells (arrow). (*C*) Distribution of the firing index F during UP states. F index = FR(DES)-FR(SWS)/FR(DES)+FR(SWS), where FR is the mean firing rate. Plus marks represent the centers of the two clusters determined by two-means cluster analysis. The boundary is shown by a dotted line. Best-fit regression line is shown.

that in all cases their spike trains were strongly locked to spindles and the K-complexes at the beginning of the UP states (Fig. S4). K-complexes consist of a sharp high-amplitude negative deflection in the electroencephalogram that reflects a synchronous excitation of cortical neurons. They originate from spontaneous activity in the cortex, which then engages the thalamo-cortical network (29). Most FSi receive abundant excitatory inputs from nearby projection cells (see *SI Methods*), and some also receive direct thalamocortical inputs (3, 17). Therefore, during SWS, bursting FSi might receive direct inputs from both the cortical circuit and the thalamus. Consistent with this, during DES segments, where spindles and K-complexes are absent, bursting activity was reduced or abolished.

Distinct Phase Modulation of Early and Late FSi by Spindle and Gamma Waves. Many FSi discharged rhythmically with spindle (7–14 Hz) and gamma (30–80 Hz) oscillations (Fig. 3*A*). Twenty-five of 45 cells (55.5%) were phase-modulated by spindles, whereas almost all, 33 of 36 (91.6%), were coupled to gamma. Interestingly, early and late populations were differently synchronized with both bands. Early cells were phase-locked to spindle troughs, whereas late FSi fired during the ascending phase of the cycle (delayed to the trough; examples in Fig. 3*B*). Remarkably, mean-phase angles relative to spindle troughs shifted progressively between the two groups and thus correlated with the firing time during UP states (Fig. 3*C*; $P = 0.086$, $n = 25$). Moreover, early FSi discharged preferentially during the descending phase of gamma cycles (advanced to the troughs), whereas late units fired at or after the troughs (Fig. 3*B*). There was also a progressive shift of mean phase angles to gamma troughs between early and late populations that correlated with the UP-state firing time (Fig. 3*C*; $P = 0.011$, $n = 33$). For each neuron, we also quantified the depth of the modulation by measuring the length of the normalized vector r (see *Materials and Methods*) that varies inversely with the amount of dispersion, and can range from 0 (uniform distribution) to 1 (identical phase angles) (44). The depth of spindle modulation decreased along UP states, revealing that the earlier a unit spikes during UP states, the stronger it is coupled to spindles ($P = 0.014$, $n = 25$). In contrast, neurons strongly modulated by gamma waves were distributed all along UP states (Fig. 3*D*; $P = 0.933$, $n = 33$).

To further assess the relationship between FSi firing and ongoing network activity, we computed spike-triggered averages of the local field potential (LFP) filtered at spindle or gamma frequencies and measured the time lag between the spike and the largest trough of the average (examples in Fig. 4*A Upper*). The averages confirmed that early cells systematically discharged earlier in time than late cells within spindle and gamma waves. Firing distributions of the same neurons around spindle and gamma troughs further corroborated these results (Fig. 4*A Lower*). More importantly, both phase differences (angular lags) and time lags of the spikes to the troughs of spindle and gamma cycles were strongly correlated in each cell (Fig. 4*B*; $P < 0.001$ each, $n = 22$), suggesting a cross-frequency coupling between the oscillations.

Discussion

This study reports the existence of two functional populations of FSi in the rat frontal cortex defined by their activity during cortical oscillations. FSi consistently discharged early or late within UP states throughout the recording session, sometimes up to 20 min (≈1,700 consecutive UP states at 0.7 Hz). This strongly suggests that the observed temporal patterns of discharge were maintained for long periods of time during SWS. These results are consistent with the observation that spontaneous neuronal activity in the neocortex propagates in stereotypical spatiotemporal sequences during SWS, each neuron exhibiting a unique temporal pattern (27).

Table 1. Differences between early and late neocortical FSi and pyramidal neurons

	Early FSi	Late FSi	All Fsi	Pyramidal
Total *n*	31	19	50	72
mPFC *n*	2	2	4	24
SMA *n*	29	17	46	48
AP width, ms	0.81 ± 0.13	0.84 ± 0.13	0.83 ± 0.12	1.23 ± 0.26***
AP amp, mV	1.67 ± 0.98	1.42 ± 0.78	1.60 ± 0.90	2.13 ± 1.1**
AP/s SWS	4.31 ± 5.01	3.33 ± 3.32	4.06 ± 4.56	2.09 ± 2.27**
AP/s DES	1.37 ± 1.23	10.81 ± 9.99**	6.06 ± 9.1	4.8 ± 6.19
Burst (B), %	10 (3)	0 (0)	6 (3)	61.1 (44)
B length, ms	9.28 ± 0.06	—	9.28 ± 0.06	7.9 ± 1.2*
B ISI, ms	3.79 ± 0.06	—	3.79 ± 0.06	3.7 ± 0.4
B frequency, Hz	264 ± 4.44	—	264 ± 4.44	269 ± 25
Percentage spikes in B	40 ± 3.6	—	40 ± 3.6	39 ± 22
AD delay, ms	—	—	—	13 ± 6

All FSi recorded were classified into early or late populations based on an UP-state firing time boundary established by cluster analysis of the 35 units for which F index and UP-state firing time could be computed.
*Late vs. early, unpaired *t*-test. Pyr vs. FSi, Mann–Whitney *U*-test. AD, antidromic response; AP, action potential; ISI, interspike interval; mPFC, medial prefrontal cortex; SMA, secondary motor area; *n*, number of cells. Mean ± SD.

An important finding of our study is that early FSi tended to be silent during epochs of DES, whereas late FSi markedly increased their discharge frequency (Table 1). We believe that late FSi may be responsible for generating the fast rhythms associated with cognitive tasks during wakefulness. In contrast, early FSi may play a role engaging neocortical networks during sleep, leading to memory consolidation.

Early FSi were better coupled to spindles than were late FSi, whereas neurons in both populations were strongly phase-locked to gamma waves. Remarkably, phase angles to spindle and gamma troughs shifted progressively between early and late cells and correlated with their UP-state firing times (i.e., early units always discharged earlier than late units within the cycles). It is important to notice that, because of the distinct location of early and late FSi in the cortical layers and the temporal distance between their discharges within UP states, it is unlikely that neurons belonging to different patterns fired during the same cycles of the ongoing oscillations (Fig. S5). We hypothesize that the phase angle shifts along UP states reflect a progressive change in the level of synchronized inputs reaching each neuron at different times of the UP state. Previous studies have proposed a dynamic spike-generating mechanism that allows detection of coincident inputs (30, 31). In terms of phase information, neurons with stronger and more synchronous excitatory drive will fire earlier in the cycle (32–34). We reasoned that pyramidal neurons coupled to spindle oscillations on the first half of UP states might send highly synchronous excitatory inputs to early FSi, promoting their early discharge within spindle and gamma waves. In agreement, it has been reported that spindles are abundant at the beginning of UP states and often follow K complexes (35). We confirmed this by calculating the probability of spindle occurrence relative to the onset of UP states and found that there is enrichment in the total number of spindle cycles within the first ≈150 ms of UP states (Fig. S4).

Furthermore, both angular and time lags for spikes relative to the troughs of spindle and gamma cycles were strongly correlated. Although spindle and gamma rhythms coexist during UP states (35), it is yet unclear whether coupling between these two bands modulate the timing of neuronal firing. Our results strongly suggest this may be the case. Although a detailed examination of this phenomenon is challenging and beyond the scope of the present study, recent findings from the human neocortex show a cross-frequency coupling between high gamma waves (30–150 Hz) and theta oscillations (5–8 Hz), in which the power of gamma oscillations was modulated during the course of a theta cycle in a behaviorally dependent manner (36). Therefore, the interplay between spindle and gamma oscillations suggested by our data may have important functional implications for cognitive processes.

Based on our present results and findings reported by others, we propose that thalamocortical spindles synchronize early FSi and pyramidal neurons in the neocortex to the spindle band to initiate and promote neuronal network activity on the first half of UP states. A cluster of early FSi, perhaps led by few bursting neurons with direct thalamic inputs, may initiate gamma waves that propagate locally. Indeed, neocortical FSi receive convergent thalamic inputs (3, 17, 37) and, during UP states, they tend to discharge earlier than regular-spiking neurons (38). Subsequently, this population of FSi may promote the establishment of gamma oscillations in deeper layers of the neocortex through chemically and/or electrically coupled networks (3, 39), which provide synchronized inhibitory potentials during UP states (40, 41). In accordance, *in vitro* studies have suggested that spontaneous recurrent activity in the neocortex is mediated by intracortical circuits (17, 18). We further hypothesize that late FSi may maintain gamma oscillations later during UP states after thalamocortical drive (and spindle generation) has subsided (Fig. S5).

Taken together, our results suggest the existence of a precise spatiotemporal pattern of neocortical FSi activity during UP states, whereby information rapidly flows between early and late neurons, initially promoted by thalamic spindles and extended efficiently in the cortex by local gamma oscillations. These results may help to elucidate the significance of gamma and spindle oscillations during natural sleep and to unravel the network alterations observed in severe psychiatric disorders such as schizophrenia.

Materials and Methods

Animals. The present experiments were approved by the Animal Research Committee of the Okazaki National Research Institutes. Male VGAT-Venus line A transgenic rats (2) weighting 250–350 g were used. VGAT-Venus rats have fluorescent labeling of nearly all cortical GABAergic cells. The animals were anesthetized with chloral hydrate (initial dose 400 mg/kg, i.p.; supplemental doses 80 mg/kg, i.v. through the femoral vein every ≈45 min) and placed in a stereotaxic frame. Body temperature was maintained at 37°C throughout the experiment with a heating pad. Lidocaine was used at all wound margins and points of contact between the animal and the stereotaxic equipment to reduce any incidental pain. The electrocorticogram (ECoG), intracortical LFP, and animal movement were monitored carefully. At the end of each cycle of anesthesia, we recorded an extra 10–20 s during which the

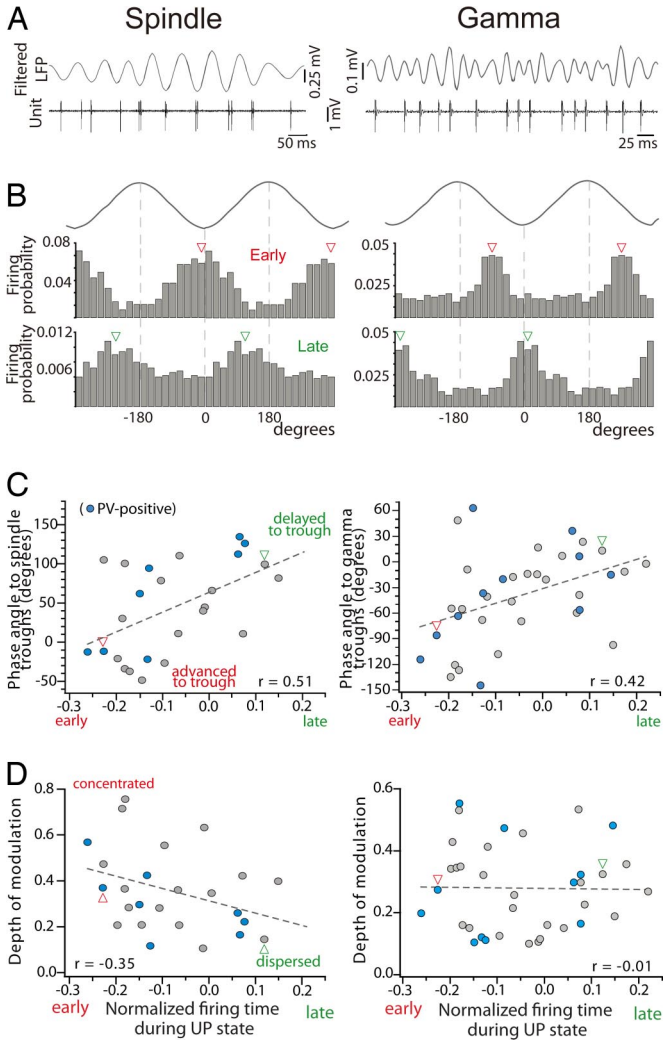

Fig. 3. Early FSi fire earlier than late FSi within spindle and gamma cycles. (*A*) Example of an early cell firing rhythmically with spindle and gamma bands (digitally filtered from the LFP). Note different time scales. (*B*) Firing probability distributions of the unit shown in *A* (*Middle*) and a late FSi (*Bottom*) during spindle and gamma cycles (*Top*). Arrowheads point to mean phase angles. Note the smaller scale for the late unit in *Left*, depicting a weak coupling to spindles. Cycles are shown twice for clarity. (*C*) Correlation of mean phase angles during spindle and gamma cycles with firing time during the UP states. Firing of early units precedes that of late units around spindle and gamma troughs. Arrowheads point to the examples shown in *B*. (*D*) Distribution of the depth of modulation during UP states. Best-fit regression lines are shown.

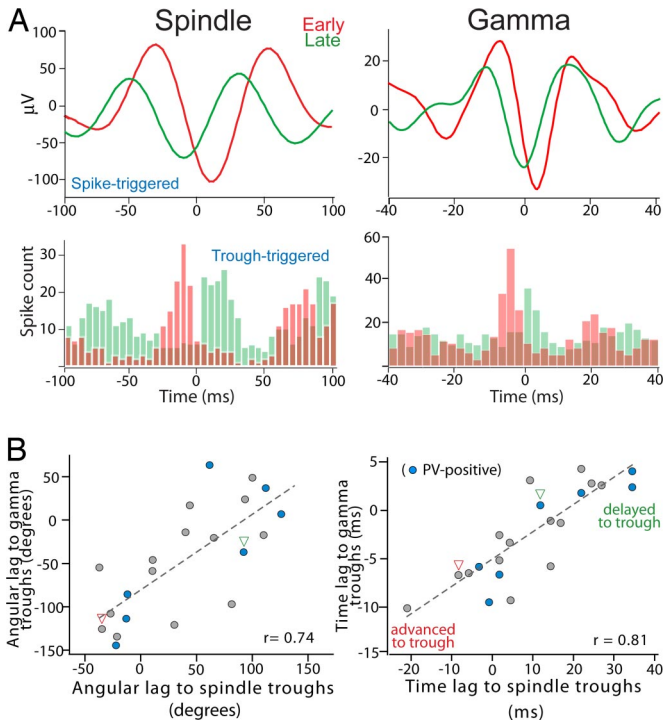

Fig. 4. Correlation between phase preferences to spindle and gamma waves. (*A Upper*) Spike-triggered averages of LFPs filtered at spindle and gamma bands. Examples of an early (red) and a late (green) FSi are shown. (*Lower*) Firing distributions of the same units around spindle and gamma troughs. Bin size, 2.5 ms. (*B*) Mean angular (*Left*) and time (*Right*) lags from spikes to spindle and gamma troughs are highly correlated. Best-fit regression lines are shown ($P < 0.001$ for both). Arrowheads point to the examples shown in *A*.

animals did not show any sign of consciousness, despite having desynchronized LFPs (DES epochs, indicated by a total cessation of slow waves and the absence of spindles). Immediately after DES epochs, animals were given a supplemental dose of anesthetic that generated slow oscillations within a few seconds. Typically, FSi were recorded during two consecutive cycles to assess changes in firing frequency during DES segments.

Electrophysiology: Single-Unit, LFP/ECoG Recordings and Electrical Stimulation. Single-unit (sampling rate 8 kHz) and LFP (sampling rate 400 Hz) activity was recorded with Spike2 software (Cambridge Electronic Devices) in the anterior cingulate and prelimbic regions of the medial prefrontal cortex (AP + 3.2, L ± 0.5, DV −1–3.5 mm from bregma) and within the secondary motor area (rostral medial agranular cortex; AP + 3.2, L ± 1.5, DV −0.5–2 mm). Recordings were made with glass pipettes (15–50 MΩ) filled with 2% neurobiotin in 0.5 M NaCl. Unit and LFP signals were filtered online at 0.3–3 kHz and 0.1–200 Hz, respectively. ECoG activity (sampling rate 400 Hz), which was recorded on the left frontal cortex via a small metal screw that crossed the skull and gently touched the dura (AP + 5.2, L −2, DV 0 mm), was filtered online at 0.1–200 Hz. Two bipolar stimulating electrodes were stereotaxically implanted in each animal, one in the dorsal striatum (AP + 0.5, L + 3, DV −5 mm) and the other in the dorsal raphe (DR, AP −7.8, L 0, DV −6.5). Stimulating electrodes consisted of two stainless steel enamel-coated wires (California Fine Wire). Stimulations were monophasic square wave pulses of 0.2 ms at 1 Hz (0.1–1 mA).

Labeling, Histology, and Immunohistochemistry. At the end of the recording session, the neurons were stained with a juxtacellular injection of neurobiotin using 500-ms cycles of positive current pulses (200 ms on/300 ms off, <8 nA) (42). Rats were perfused with fixative 2–4 h after labeling and the brain removed and kept in fixative overnight. The brain was then sliced, and the position of the stimulating electrodes confirmed after Nissl staining. Frontal sections were processed for neurobiotin (visualized with Alexa Fluor 350 avidin). Neurobiotin-positive neurons that were also Venus-positive (interneurons) were postprocessed for PV immunoreactivity (visualized with Alexa Fluor 594 secondary antibody). Thirteen neurons were successfully stained with neurobiotin and positive for Venus and PV, one in the medial prefrontal cortex and 12 in the secondary motor area. We reconstructed three late FSi with Neurolucida that exhibited basket cell-like morphology (Fig. S1). In addition, another 7 units sufficiently stained with neurobiotin were also found to be Venus-positive (and thus were interneurons); however, PV immunoreactivity could not be examined in these cells.

Identification of FSi in VGAT-Venus Transgenic Rats *in Vivo*. We electrically stimulated the striatum and dorsal raphe to identify projection neurons by antidromic activation. When we compared the *in vivo* firing patterns of the 13 PV-positive FSi stained with neurobiotin with pyramidal neurons identified by antidromic activation, we found that FSi were identifiable by a number of features: (*i*) they displayed very brief action potentials, (*ii*) they fired at much higher frequencies during the depolarizing pulses used for staining, and (*iii*) they were activated by feedforward inputs from pyramidal cells projecting to dorsal raphe and/or striatum. See *SI Methods* Figs. S1 and S2, and Table S1 for a detailed explanation. These unique characteristics allowed confident iden-

tification of an additional 37 nonrecovered FSi that have been included in our results.

Data Analysis. The start and end of the UP states were determined by measuring changes in the 20- to 100-Hz component of the LFP, following a method proposed by Mukovski *et al.* (43). Spindle (7–14 Hz) and gamma (30–80 Hz) bands were digitally filtered in Spike2 and big troughs detected with PTLEV script. For each cell, we built phase histograms (20° bin) of spike-timing relative to spindle/gamma troughs, and firing was considered modulated by the oscillation if $P < 0.05$ using the Raleigh test. Firing probabilities were calculated by normalizing the number of spikes in each bin by the total number of cycles. From the phase histograms, we computed the mean angle and the depth of the modulation *r*, which was the length of the mean vector sum of all phase angles normalized by the number of spikes/angle (44). To improve accuracy, time lags between spikes and gamma negativity were computed by curve-fitting a 4-degree polynomial function (least-squares method) to the negative points of the spike-triggered averages. Neurons that contaminated the LFPs with the spikes were not used for circular analysis ($n = 17$).

Orthodromic and antidromic activations of FSi and pyramidal neurons after striatal and raphe electrical stimulation, respectively, were analyzed by using peristimulus histograms (bin = 2 ms) built in Spike2 (45). Briefly, orthodromic excitations elicited spikes with short and variable latencies, and poststimulus discharge rates significantly greater than the mean baseline firing rate (200 ms before the stimulus) plus two times its standard deviation for at least four consecutive bins. Antidromic excitations induced spikes at a fixed latency until a spontaneous occurring spike provoked a collision. The success rate of the excitations was computed as the firing rate during excitation divided by the firing rate during baseline.

Basic statistical analysis was performed by using SPSS. Circular statistics, LFP processing (to detect UP-state start/end), and curve fitting were computed in MATLAB (The MathWorks). Data are expressed as mean ± standard deviation. Statistical significance was set at a 95% confidence level (two-tailed).

ACKNOWLEDGMENTS. We thank A. T. Gulledge and M. Bosch for discussion and comments on this manuscript. We are grateful to M. Saito and Y. Ito for excellent technical assistance. We thank Y. Hirai and the Center for Experimental Animals [National Institute for Physiological Sciences (NIPS)] for breeding and genotyping the transgenic line. VGAT-Venus transgenic rats were generated by Y. Yanagawa, M. Hirabayashi, and Y. Kawaguchi at the NIPS, using pCS2-Venus provided by A. Miyawaki. This work was supported by Grants-in-Aid for Scientific Research from the Ministry of Education, Culture, Sports, Science and Technology (MEXT) and the Ministry of Health, Labor and Welfare of Japan. M.V.P. was supported by a postdoctoral fellowship from the Japan Society for the Promotion of Science (JSPS Grant PE04061).

1. Kawaguchi Y, Kubota Y (1997) GABAergic cell subtypes and their synaptic connections in rat frontal cortex. *Cereb Cortex* 7:476–486.
2. Uematsu M, *et al.* (2008) Quantitative chemical composition of cortical GABAergic neurons revealed in transgenic Venus-expressing rats. *Cereb Cortex* 18:315–330.
3. Gibson JR, Beierlein M, Connors BW (1999) Two networks of electrically coupled inhibitory neurons in neocortex. *Nature* 402:75–79.
4. Hestrin S, Galarreta M (2005) Electrical synapses define networks of neocortical GABAergic neurons. *Trends Neurosci* 28:304–309.
5. Bartos M, Vida I, Jonas P (2007) Synaptic mechanisms of synchronized gamma oscillations in inhibitory interneuron networks. *Nat Rev Neurosci* 8:45–56.
6. Howard MW, *et al.* (2003) Gamma oscillations correlate with working memory load in humans. *Cereb Cortex* 13:1369–1374.
7. Singer W (1999) Neuronal synchrony: A versatile code for the definition of relations? *Neuron* 24:49–65.
8. Lewis DA, Hashimoto T, Volk DW (2005) Cortical inhibitory neurons and schizophrenia. *Nat Rev Neurosci* 6:312–324.
9. Spencer KM, *et al.* (2003) Abnormal neural synchrony in schizophrenia. *J Neurosci* 23:7407–7411.
10. Cho RY, Konecky RO, Carter CS (2006) Impairments in frontal cortical gamma synchrony and cognitive control in schizophrenia. *Proc Natl Acad Sci USA* 103:19878–19883.
11. Steriade M, Contreras D, Amzica F, Timofeev I (1996) Synchronization of fast (30–40 Hz) spontaneous oscillations in intrathalamic and thalamocortical networks. *J Neurosci* 16:2788–2808.
12. Steriade M, Amzica F, Contreras D (1996) Synchronization of fast (30–40 Hz) spontaneous cortical rhythms during brain activation. *J Neurosci* 16:392–417.
13. Steriade M, McCormick DA, Sejnowski TJ (1993) Thalamocortical oscillations in the sleeping and aroused brain. *Science* 262:679–685.
14. Contreras D, Destexhe A, Steriade M (1997) Intracellular and computational characterization of the intracortical inhibitory control of synchronized thalamic inputs *in vivo*. *J Neurophysiol* 78:335–350.
15. Sejnowski TJ, Destexhe A (2000) Why do we sleep? *Brain Res* 886:208–223.
16. Kawaguchi Y, Kubota Y (1998) Neurochemical features and synaptic connections of large physiologically-identified GABAergic cells in the rat frontal cortex. *Neuroscience* 85:677–701.
17. Beierlein M, Fall CP, Rinzel J, Yuste R (2002) Thalamocortical bursts trigger recurrent activity in neocortical networks: layer 4 as a frequency-dependent gate. *J Neurosci* 22:9885–9894.
18. MacLean JN, Watson BO, Aaron GB, Yuste R (2005) Internal dynamics determine the cortical response to thalamic stimulation. *Neuron* 48:811–823.
19. Marshall L, Helgadóttir H, Mölle M, Born J (2006) Boosting slow oscillations during sleep potentiates memory. *Nature* 444:610–613.
20. Stickgold R (2005) Sleep-dependent memory consolidation. *Nature* 437:1272–1278.
21. Buzsáki G (1989) Two-stage model of memory trace formation: A role for ''noisy'' brain states. *Neuroscience* 31:551–570.
22. Battaglia FP, Sutherland GR, McNaughton BL (2004) Hippocampal sharp wave bursts coincide with neocortical ''up-state'' transitions. *Learn Memory* 11:697–704.
23. Mölle M, *et al.* (2006) Hippocampal sharp wave-ripples linked to slow oscillations in rat slow-wave sleep. *J Neurophysiol* 96:62–70.
24. Sirota A, Csicsvari J, Buhl D, Buzsáki G (2003) Communication between neocortex and hippocampus during sleep in rodents. *Proc Natl Acad Sci USA* 100:2065–2069.
25. Siapas AG, Wilson MA (1998) Coordinated interactions between hippocampal ripples and cortical spindles during slow-wave sleep. *Neuron* 21:1123–1128.
26. Ji D, Wilson MA (2007) Coordinated memory replay in the visual cortex and hippocampus during sleep. *Nat Neurosci* 10:100–107.
27. Luczak A, *et al.* (2007) Sequential structure of neocortical spontaneous activity *in vivo*. *Proc Natl Acad Sci USA* 104:347–352.
28. Nowak LG, *et al.* (2003) Electrophysiological classes of cat primary visual cortical neurons *in vivo* as revealed by quantitative analyses. *J Neurophysiol* 89:1541–1566.
29. Amzica F, Steriade M (2002) The functional significance of K-complexes. *Sleep Med Rev* 6:139–149.
30. Azouz R, Gray CM (2003) Adaptive coincidence detection and dynamic gain control in visual cortical neurons *in vivo*. *Neuron* 37:513–523.
31. Azouz R (2005) Dynamic spatiotemporal synaptic integration in cortical neurons: Neuronal gain, revisited. *J Neurophysiol* 94:2785–2796.
32. Buzsáki G, Chrobak JJ (1995) Temporal structure in spatially organized neuronal ensembles: a role for interneuronal networks. *Curr Opin Neurobiol* 5:504–510.
33. Buzsáki G, Draguhn A (2004) Neuronal oscillations in cortical networks. *Science* 304:1926–1929.
34. Volgushev M, Chistiakova M, Singer W (1998) Modification of discharge patterns of neocortical neurons by induced oscillations of the membrane potential. *Neuroscience* 83:15–25.
35. Steriade M (2006) Grouping of brain rhythms in corticothalamic systems. *Neuroscience* 137:1087–1106.
36. Canolty RT, *et al.* (2006) High gamma power is phase-locked to theta oscillations in human neocortex. *Science* 313:1626–1628.
37. Porter JT, Johnson CK, Agmon A (2001) Diverse types of interneurons generate thalamus-evoked feedforward inhibition in the mouse barrel cortex. *J Neurosci* 21:2699–2710.
38. Volgushev M, Chauvette S, Mukovski M, Timofeev I (2006) Precise long-range synchronization of activity and silence in neocortical neurons during slow-wave sleep. *J Neurosci* 26:5665–5672.
39. Galarreta M, Hestrin S (2002) Electrical and chemical synapses among parvalbumin fast-spiking GABAergic interneurons in adult mouse neocortex. *Proc Natl Acad Sci USA* 99:12438–12443.
40. Hasenstaub A, *et al.* (2005) Inhibitory postsynaptic potentials carry synchronized frequency information in active cortical networks. *Neuron* 47:423–435.
41. Rudolph M, Pospischil M, Timofeev I, Destexhe A (2007) Inhibition determines membrane potential dynamics and controls action potential generation in awake and sleeping cat cortex. *J Neurosci* 27:5280–5290.
42. Pinault D (1996) A novel single-cell staining procedure performed *in vivo* under electrophysiological control: Morpho-functional features of juxtacellularly labeled thalamic cells and other central neurons with biocytin or neurobiotin. *J Neurosci Methods* 65:113–136.
43. Mukovski M, Chauvette S, Timofeev I, Volgushev M (2007) Detection of active and silent states in neocortical neurons from the field potential signal during slow-wave sleep. *Cereb Cortex* 17:400–414.
44. Zar JH (1999) *Biostatistical Analysis* (Prentice–Hall, Upper Saddle River, NJ).
45. Puig MV, Artigas F, Celada P (2005) Modulation of the activity of pyramidal neurons in rat prefrontal cortex by raphe stimulation *in vivo*: Involvement of serotonin and GABA. *Cereb Cortex* 15:1–14.